Application of CEEMDAN in Analyzing Cosmic Ray Properties before Great Geomagnetic Storms

Qian Ye[1], Cong Wang[2], and bingsen xue[3]

[1]National Satellite Meteorological Center
[2]National Satellite Meteorological Center , CMA
[3]National satellite meteorologic center

November 21, 2022

Abstract

The short-term disturbance of galactic cosmic rays(GCRs) caused by coronal cass ejections (CMEs) can be quantified to indicators of geomagnetic storms. We proposed a model takes GCRs time series slice as input and generates two geomagnetic storm prediction indexes as output. This new model is based on Hilbert-Huang Transform (HHT), utilizing Complete Ensemble Empirical Mode Decomposition with Adaptive Noise (CEEMDAN) instead of Empirical Mode Decomposition (EMD), and extends 2D spectrum result of HHT to 3D form.Two prediction indexes is constructed from the sensitive components in GCRs. Finally, this model is tested on 11 great geomagnetic storms(Kp>=8) during solar cycle 23 and 24. Accuracy of this model turned out to be 82%, and prediction lead time ranges from 9 to 24 hours.

Application of CEEMDAN in Analyzing Cosmic Ray Properties before Great Geomagnetic Storms

Cong Wang[1,2]**,Qian Ye**[1,2]**,BingSen Xue**[1,2]

[1]Key Laboratory for Space Weather, National Center for Space Weather, Beijing 100081, China
[2]National Satellite Meterological Center, Beijing 100081, China

Key Points:

- CEEMDAN is a robust method for time series decomposition.
- 3D spectrum of GCRs is an useful tool for monitoring disturbance in geomagnetic field.
- Two indexes basing on IMFs are proposed in this paper, and proven to be accurate precursors of geomagnetic storm.

Corresponding author: Qian Ye, `yeqian@cma.gov.cn`

Abstract

The short-term disturbance of galactic cosmic rays(GCRs) caused by coronal cass ejections (CMEs) can be quantified to indicators of geomagnetic storms. We proposed a model takes GCRs time series slice as input and generates two geomagnetic storm prediction indexes as output. This new model is based on Hilbert-Huang Transform (HHT), utilizing Complete Ensemble Empirical Mode Decomposition with Adaptive Noise (CEEMDAN) instead of Empirical Mode Decomposition (EMD), and extends 2D spectrum result of HHT to 3D form.Two prediction indexes is constructed from the sensitive components in GCRs. Finally, this model is tested on 11 great geomagnetic storms($Kp \geq 8$) during solar cycle 23 and 24. Accuracy of this model turned out to be 82%, and prediction lead time ranges from 9 to 24 hours.

1 Introduction

Geomagnetic storms are significant space weather events, and great geomagnetic storms($Kp \geq 7$) could damage satellites , affect VLF signal propagation and electric potential of power distribution network (Dorman, 2005; Starodubtsev et al., 2019; Liu & Wan, 2014). Meanwhile, great geomagnetic storms can cause ionospheric disturbance (Kravtsova & Sdobnov, 2016; Mandrikova et al., 2018), magnetospheric disturbance (Manninen et al., 2008) and even threat aviation passenger's health. Hence, accurate and timely prediction of great geomagnetic storms can minimize the potential loss. Interaction between the southward component of interplanetary magnetic field in solar wind and the the magnetosphere of Earth is thought to be the main source of geomagnetic storms (Liu & Wan, 2014). Galactic cosmic rays(GCRs), which contain information about disturbance in interplanetary space, (Belov et al., 2003; Kichigin et al., 2017), can be a precursor of great geomagnetic storm. GCRs are energetic charged particles originated outside the solar system, which are modulated by magnetic field of the Earth, the Sun and the solar wind (Mandrikova et al., 2018; Kravtsova & Sdobnov, 2016). As described earlier, information reflecting intensity of the disturbance in interplanetary space is hidden in features of GCRs' flux and anisotropy. The information mirrors both periodic component include different length periodicities from 9.5 months to 19 years(Otaola et al., 1985; Valdés-Galicia et al., 1996; Tsichla et al., 2019) and aperiodic component, which is mainly caused by coronal mass ejections(CMEs). CMEs are gigantic magnetized plasma clouds ejected from the sun's corona, also main source of extreme space weather, especially great geomagnetic storm (Kilpua et al., 2019). Zhang et al. (2007) pointed out that between 1996 and 2005, 60% of Major Geomagnetic Storms were associated with an individual CME, and 27% of them were influenced by multiple CMEs. Shi et al. (2014) obtained similar conclusion after investigating all moderate and strong geomagnetic storms between 2007 and 2012. It's worth noting that most of the geomagnetic storms are accompanied by transient decreases in cosmic ray intensity. Work of Starodubtsev et al. (2019) indicates GCRs is a predictor of geomagnetic storm whose lead time from a few hours to 1.5 days.

Many authors have realized extracting corresponding disturbance of GCRs can improve the accuracy of forecasting. (Dorman, 1999; Munakata et al., 2000; Kudela et al., 2001, 2000; Dorman, 2005; Xue, 2007; Zhu et al., 2015).Dorman (1999) pointed there was changes and appearance of peaks at some frequencies in GCRs' frequency spectrum before geomagnetic storms. Subsequently, Munakata et al. (2000) systematically investigated GCRs as precursor of geomagnetic storms firstly. They analyzed a total of 39 geomagnetic storms between 1992 and 1998, then found GCRs precursors will appear 6-9 hours ahead of geomagnetic storms. By means of analyzing one-hour GCRs intensity, Dorman (2005) suggested that Forbush-decrease in GCRs is a precursor of geomagnetic storms with 10-15 hours forecast lead. Xue (2007) utilized an algorithm acquired precursor by calculating deviation between GCRs flux of specific moment and CRs average flux, finally, the algorithm's precision reached 80% by testing on data of 2001. Zhu

et al. (2015) employed morlet wavelet to extract the abnormal fluctuations of CR before great geomagnetic storms, successfully increasing forecast lead to 12 hours.

At present, most attempts that forecasting geomagnetic storms based on GCRs are scientific research, therefore these works care more about relationship between GCRs and geomagnetic storm than efficient forecasting. In examples mentioned above, either the time span of training data is too short, or the final result is not a clear indicator. So in this study, a new model is proposed, which focus on extracting and quantifying the information related to geomagnetic storms in GCRs to forecasting extreme geomagnetic storms caused by CMEs. Complete Ensemble Empirical Mode Decomposition with Adaptive Noise is utilized to obtaining sporadic fluctuation of GCRs. Then Hilbert Transform is employed to converting signal from time-domain to frequency-domain, in order to amplifying the disturbance caused by CME. Our model takes 4-day GCRs flux slice as input, meanwhile generates a 3D spectrum and two prediction indexes forecasting extreme geomagnetic storms (Kp$\geq$8) as output.

Description of methodology is in Section 2, and data details is given in Section 3. Results and the analysis of them are shown in Section 4. In Section 5, we summarize findings during research and discuss deficiencies of our model and propose future improvement plans.

2 Methodology

In this study, GCRs observation is splitted in this way: data is segmented into 4-day long slice along time, and the interval between two slices is half-hour. The choice of 4 days as the slice length is based on the fact that CME propagation time (from the Sun to the Earth) is usually 3 days, The half-hour interval is a comprehensive consideration of timeliness of forecasting and efficiency of computation. CMEs are known to be an important cause of intense geomagnetic disturbances. GCRs can catch CME's arrival, for this reason, it can be an indicator of geomagnetic storms cause by CMEs. While except CMEs, GCRs is modulated by many other factors with different modulation cycles. Tsichla et al. (2019) obtained several main cycles from GCRs time series during 1965–2018 by spectrum analysis, such as 9.5 months, 1.2 years and so on. Long-term factors (more than 2 years) are easier to spot, for example, solar activity is foremost long-term factorTomassetti et al. (2017). It is clear that GCRs and sunspot numbers all have 10-year periods. Mid-term cycles (more than 1 month, less than 2 years) is more complex. The 1.1-year periodicity is due to the Earth's orbit around the Sun, and the 7.2-year periodicity is probably related to the magnetic cycle. Short-term cycles (less than 1 month) is even more complicated, because GCRs' short-term observation is combined action of long-term, mid-term and short-term components.

Using short-term GCRs observation to real-time forecasting is a challenge. Dividing GCRs into components with different cycle lengths will simplify this problem, therefore signal processing is a good solution for this problem. Traditional signal processing methods include time-domain and frequency-domain methods. Time-domain methods measure max, min, mean values of a signal. It catches specific features of signal, but can not reveal the law of signal fluctuation. Frequency-domain methods decompose one signal into a sum of functions according to basis function. Fast Fourier Tansform (FFT) is the most popular frequency-domain analysis tool, whose basis function is sinusoidal signal. Through FFT, frequency components of the signal can be calculated, but their localization in the time series can not be obtained. Short Time Fourier Transform (STFT) improve this problem by introducing "time window". Another problem of both FFT and STFT is that the input signal must be stationary, but in the real world, most signals do not meet this requirement. For spectrum analysis application in the real world, in 1998, Huang.E, a scientist in NASA, proposed Hilbert Huang Transform (HHT), a modern time-frequency tool suitable for non-stationary and non-linear signals. (Huang et al., 1998)

114 HHT is actually composed of two parts: empirical mode decomposition (EMD) and
115 Hilbert Transform (HT). EMD is an adaptive time-domain signal decomposition method.
116 A signal will be divided into quasi-periodic oscillatory signal and superimposed random
117 background signal by EMD(Kolotkov et al., 2016). It decomposes a signal $X(t)$ into N
118 number of intrinsic mode functions (IMF), and residual $r_n(t)$ using the sifting process
119 (Barnhart & Eichinger, 2011). A brief overview of the sifting process is as follows:

120   1. Find local maxima and minima for signal $X(t)$ to construct an upper envelope $e_{max}(t)$,
121   and a lower envelope $e_{min}(t)$
122   2. Compute mean envelope for ith iteration, $m(t)$

$$m(t) = \frac{1}{2}[e_{max}(t) + e_{min}(t)]$$

123   3. With $c_n(t) = X(t)$ for the first iteration, subtract mean envelope from residual
124   signal

$$c_n(t) = c_n(t) - m(t)$$

125   4. The procedure is iterated again at step 1 with the new value of $c_n(t)$ if $c_n(t)$ does
126   not match the criteria of an IMF, otherwise $c_n(t)$ is a new imf, and a new resid-
127   ual signal is computed meanwhile.

$$imf_n(t) = c_n(t)$$

128

$$X(t) = X(t) - c_n(t)$$

129   5. Then begin from step 1, using the residual signal as a new signal $X(t)$

130 The process will stop when $X(t)$ becomes a monotonic function, Original signal is finally
131 represented as:

$$X(t) = r(t) + \sum_{n=1}^{N} imf_n(t)$$

132   imf_n is n_{th} intrinsic mode function, and $r(t)$ represents residual.

133 After EMD, each IMF becomes stationary and linear, then HT is utilized to ob-
134 tain frequency information of IMFs. HT is very similar to FFT, which can be simply un-
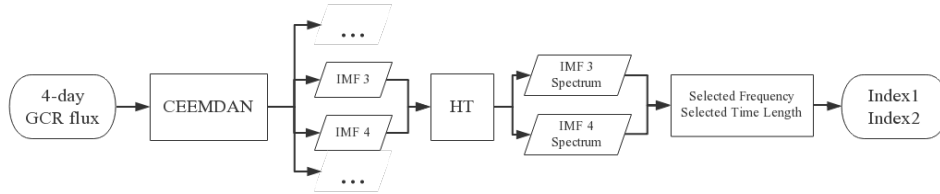135 derstood as FFT without negative frequency.

Figure 1: Flowchart of Our Model

136 Our work is illustrated in Figure 1, roughly can be divided into two parts. Firstly,
137 a new model based on HHT is proposed which has two improvements. One improvement

is replacing EMD with complete ensemble empirical mode decomposition with adaptive noise (CEEMDAN). Robustness is the reason why we choose CEEMDAN. Although EMD performs very well in dealing with non-stationary and non-linear signals (Coughlin & Tung, 2004; Barnhart & Eichinger, 2011; Käpylä, M. J. et al., 2016; Cho et al., 2016; Kolotkov et al., 2016; Stangalini et al., 2014; Xiang & Qu, 2016), it still has "mode mixing" problem. "Mode mixing" refers to the main frequency component of two IMFs is very similar. A recent improvement of EMD is ensemble empirical mode decomposition(EEMD), which uses additional noise instead of subjective selection criteria to better separate different frequency scales into different IMFs(Huang & Wu, 2008). However, the EEMD algorithm cannot completely eliminate Gaussian white noise after signal reconstruction, it cause reconstruction errors. CEEMDAN was proposed to solving this problem. In CEEMDAN, the averaging over all ensemble members is carried separately for each IMF component. This small change also seems to improve the algorithm's efficiency in recovering an underlying tone from an already noisy input signal(COLOMINAS et al., 2012). The other improvement is transforming the final presentation form of Hilbert Transform from 2D to 3D. IMF3 and IMF4 are more sensitive to geomagnetic disturbance caused by CMEs than other IMFs after Hilbert Transform . In spectrum of IMF3 and IMF4, components with periods from 9.6 to 96 hours are closely related to geomagnetic storms. By choosing this cycle range as vertical axis, and time as horizontal axis, a 3D spectrum obtained. Secondly, two prediction indexes of geomagnetic storms caused by CME is created, which take consideration of both IMF3 and IMF4.

So to summarize, our model takes slice as input, and gives an intermediate output and a final output. The intermediate output is the 3D spectrum of IMF 3 and 4. The final output is two prediction indexes.

3 Data

Table 1: CME Cases Selected from Solar Cycle 23 and 24

CME Burst Time	Mean 1 AU transit speed of CME(km/s)	Time to Earth(hour)	Geomagnetic Storm Start Time	Max Kp Index
2001-03-28	690	60.0	2001-03-28 03:00	9
2001-11-22	1330	31.4	2001-11-24 06:00	9
2003-11-18	886	47.2	2003-11-20 09:00	9
2004-11-04	720	67.0	2004-11-07 21:00	9
2005-05-13	1270	33.4	2005-05-15 06:00	9
2005-08-22	790	52.7	2005-08-24 06:00	9
2011-08-04	1100	37.6	2011-08-05 18:00	8
2011-09-24	1248	47.8	2011-09-26 15:00	8
2015-03-15	840	50.2	2015-03-17 12:00	8
2015-06-21	1040	40.0	2015-06-22 18:00	8
2017-09-06	1210	34.2	2017-09-07 21:00	8

data url: http://www.srl.caltech.edu/ACE/ASC/DATA/level3/icmetable2.htm

The geomagnetic storms caused by CMEs are selected according to Kp index in the period of 1996-2018. GCRs intensity are taken from Oulu neutron-monitor station (coordinates: 60.05°N, 25.47°E; cut-off rigidity: 0.8 GV). GCRs data is downloaded on the site: http://cosmicrays.oulu.fi/. Considering time resolution and computation speed, 30 minutes is chosen as time resolution of GCRs slice. Geomagnetic indices come in many

168 forms, each of them could represents a special phenomenon(Chandorkar et al., 2017). The
169 Kp index is a 3 h long comprehensive geomagnetic activity index, also the indicator of
170 geomagnetic activity in this work. The geomagnetic index Kp was taken from Space Weather
171 Prediction Center, Kp index data is obtained from the site: ftp://ftp.swpc.noaa.gov/pub/indices/old_indices/.

172 The six extreme geomagnetic storms(Kp≥9) during 23rd solar cycle(Zhang et al.,
173 2007; Cerrato et al., 2012) and five severe geomagnetic storms(Kp≥8) during 24rd so-
174 lar cycle(Shi et al., 2014; Wu et al., 2016; Tokumaru et al., 2019) were chosen as study
175 samples. All of these geomagnetic storms were caused by CMEs. On account of the fact
176 that the solar activity of 24rd solar cycle is lower than 23rd solar cycle. No extreme ge-
177 omagnetic storms (Kp≥9) occurred in 24rd solar cycle, hence, we choose five severe ge-
178 omagnetic storms (Kp≥8) during 24rd solar cycle as study samples. The cases selected
179 are shown in Table 1.

4 Result and Analysis

4.1 Robustness of CEEMDAN

182 Figure 2(a) shows GCRs (first row) as well as its IMFs and residual (last row) ex-
183 tracted by EMD from 2005-05-15 18:00 to 2005-05-19 18:00, Figure 2(b) displays the same
184 observations from 2005-05-16 00:00 to 2005-05-20 00:00. Those two figures show the short-
185 comings of EMD. Firstly, theoretically, the main frequency of each IMF should not change
186 much, but the frequencies of the first half and the second half of IMF 4 in Figure 2(a)
187 are visually different. The same problem occurred in IMF 4 of Figure 2(b). Secondly,
188 the main frequencies of different IMF should be distinguished, just like IMF 2 and 3 in
189 Figure 2(a). But actually, difference of IMF 3,4,5 in the same figure is slight. The same
190 thing happens in IMF 3 and 4 of Figure 2(b). Lastly, the time interval between these
191 two signals is only 6 hours. In theory, there should be no big difference between decom-
192 position results, but the number of IMFs of is 4 and 5 respectively.

193 Then CEEMDAN is tested on the same data. Figure 3(a) and 3(b) illustrates the
194 advantages of this method. Firstly, main frequency of every IMF is consistent. Secondly,
195 there is clear distinction between main frequencies of different IMF. Lastly, it guaran-
196 tee the stability of decomposition over time, the number of IMFs are both 8 in these two
197 figures.

4.2 3D Spectrum

199 Figure 4(a) is 3D spectrum during the geomagnetic storm on September 26th, 2011
200 (event1). This geomagnetic storm was caused by a CME which eruptived from AR11283
201 at N12E60 on 24 September. This CME eruptived from the active region with the lin-
202 ear speed of 1248 km/s(from the SOHO/LASCO CME catalog, cdaw.gsfc.nasa.gov/CME_list/).
203 Geomagnetic activity level before this storm is very low, as all Kp index is lower 3. Most
204 of this spectrum is very clean (low values), but there is a peak area in IMF3 around 15:00
205 on September 25th, 21 hours before event1, and a sub peak area around 21:00 on Septem-
206 ber 26th. The peak value is the target precursor of this event, and the sub peak area is
207 a chain reaction of the storm. Chain reaction is a manifestation of Forbush Decrease (Calogovic
208 et al., 2010). The same chain reaction also arises in IMF4.

209 Similarly, a peak area appeared in IMF4 of Figure 4(b), 18 hours before the geo-
210 magnetic storm on 00:00 September 8th, 2017 (event2), and the chain reaction also kept
211 up with this storm. This geomagnetic storm was caused by a full-halo CME which erup-
212 tived from AR12673 on September 6th, 2017. This active region produced 4 X-class flares
213 between 04 and 10 September 2017(Tokumaru et al., 2019). This CME eruptived from
214 the active region with the linear speed of 1571 km/s(from the SOHO/LASCO CME cat-
215 alog, cdaw.gsfc.nasa.gov/CME_list/), and associated with the 06 September X9.3 flare.
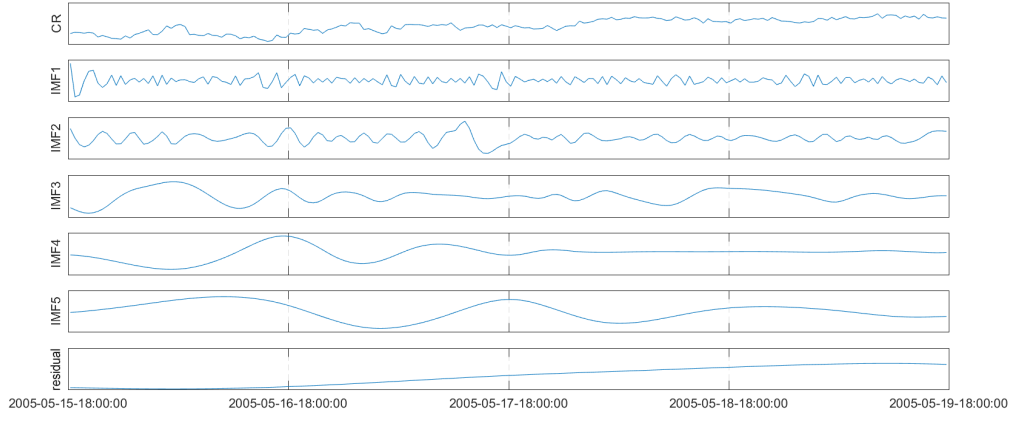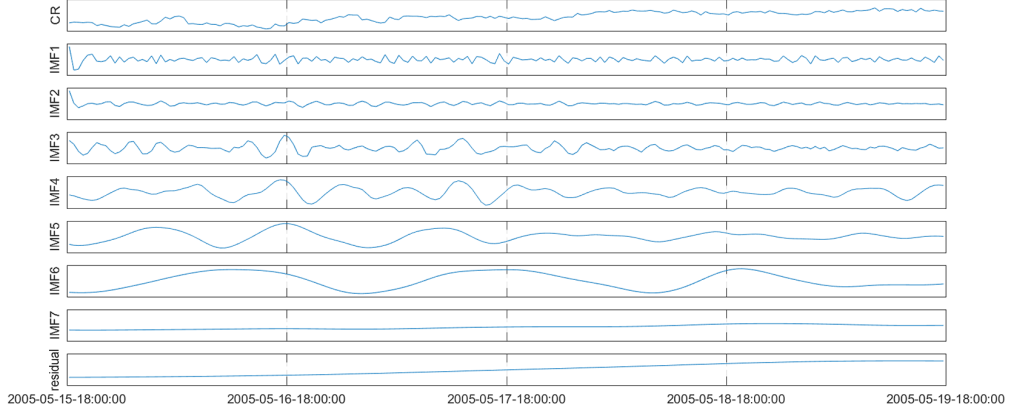
(a)
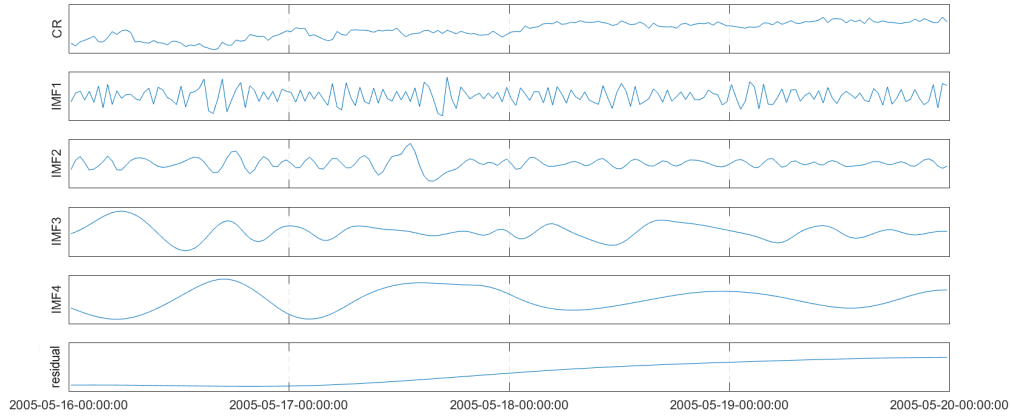
(b)

Figure 2: Galactic Cosmic Ray and its IMFs under EMD
(a)2005-05-15 18:00 to 2005-05-19 18:00 (b)2005-05-16 00:00 to 2005-05-20 00:00

According to Figure 4(b) , IMF4 spectrum is very quiet before peak area. But it's different in IMF3, there are many peak areas spreading in IMF3 spectrum. Figure 5 may explain this phenomenon. On 21:00 September 12th, 2011 (event3), there is only one individual minor geomagnetic storm (Kp=5). So there is no doubt that disturbance in IMF3 and IMF4 was affected by this minor storm. Then let's go back to Figure 4(b) again, situation in IMF3 is similar with event3, because there is a minor storm (Kp=5) happened on 21:00 September 4th, 2017.

4.3 Prediction Indexes

Figure 4(a) is a 3D spectrum. In this 3D spectrum, there is an obvious enhancement occurred in IMF4 before geomagnetic storm, implying this spectrum can be a real time monitoring tool. 3D spectrum provides a comprehensive perspective, but the information contained is not intuitive. It's more like a qualitative analysis tool than a quantitative analysis tool. We want more simple and direct indicators corresponding to geomagnetic storms. After testing on the data from 2001 to 2019, we found components with periods from 13 to 24 hours is the most sensitive elements with geomagnetic storm. Then we combine those components into two indexes, Figure 6 shows the principle of construction: Index1 and Index2 both are combination of values A and B. A equals the
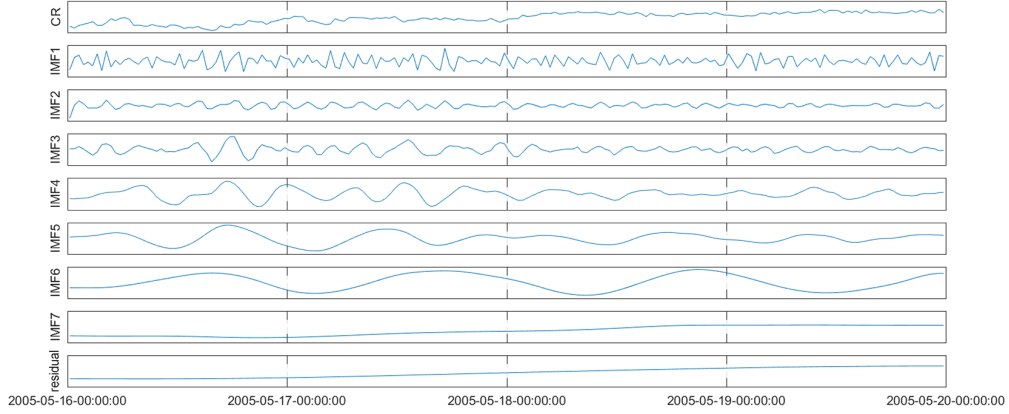
Figure 3: Galactic Cosmic Ray and its IMFs under CEEMDAN
(a)2005-05-15 18:00 to 2005-05-19 18:00 (b)2005-05-16 00:00 to 2005-05-20 00:00

sum of all values in the red box, and B equals the sum of all values in the green box. The
time width of the box is 6 hours, which is determined after large number of experiments.

The specific formula of two indexes is as follows:

$$Index1(t) = \sum_{p=13h}^{24h} \sum_{t=now-6h}^{now} (10^{-3} \times Amplitude_{imf3}(t,p) + 10^{-4} \times Amplitude_{imf4}(t,p))$$

$$Index2(t) = \sum_{p=13h}^{24h} \sum_{t=now-6h}^{now} 10^{-4} \times (Amplitude_{imf3}(t,p) + Amplitude_{imf4}(t,p))$$

The difference between two formulas is just the coefficients in front of IMF3. Fig-
ure 4(a) and 4(b) explain the reason. Fig 4(a) is the 3D spectrum of event in Septem-
ber 7, 2017. There is a noticeable enhancement in IMF3 before the magnetic storm with
a 9-hour lead time. But in Figure 4(b), which shows event in September 7, 2017, the fea-
ture appears in IMF4. This phenomenon means that the two components need to be con-
sidered at the same time. Furthermore, the magnitude of IMF3 isn't very stable, some-
times it is the same order of magnitude as IMF4, sometimes is ten times of IMF4. That's
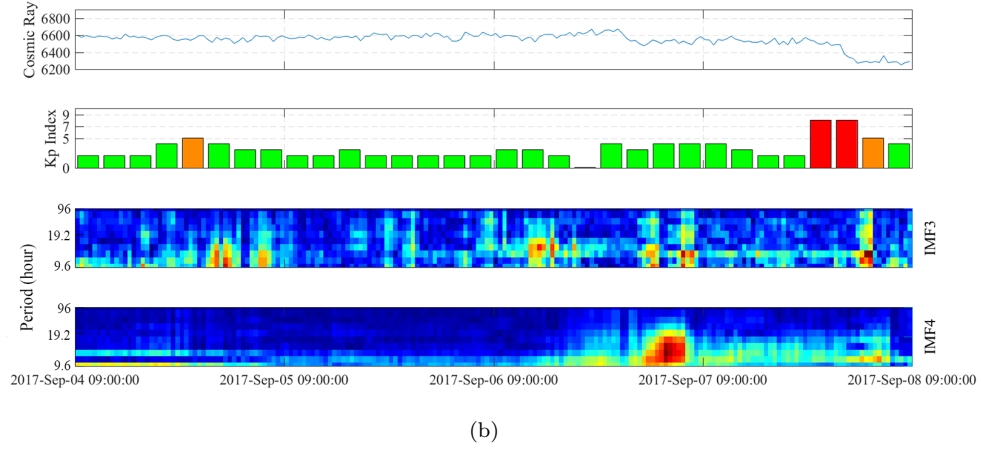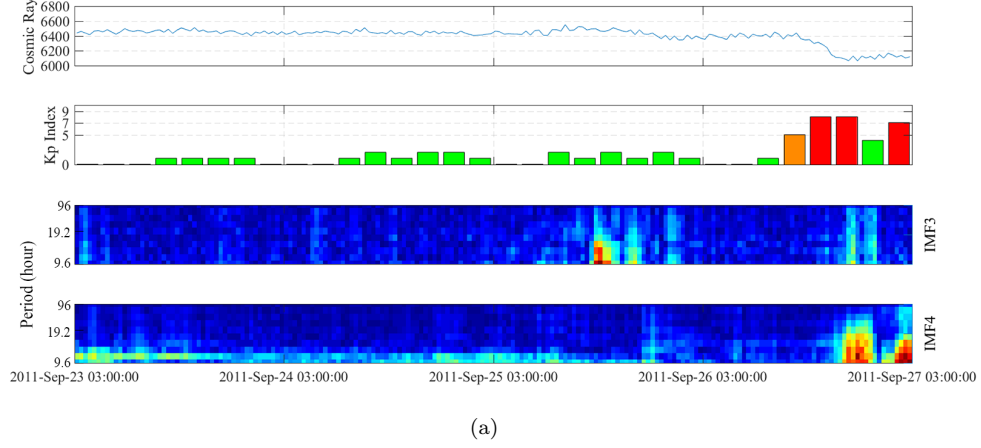
(a)

(b)

Figure 4: 3D Spectrum of event. GCRs, Kp index, IMF3, IMF4 are shown in turn from top to bottom.
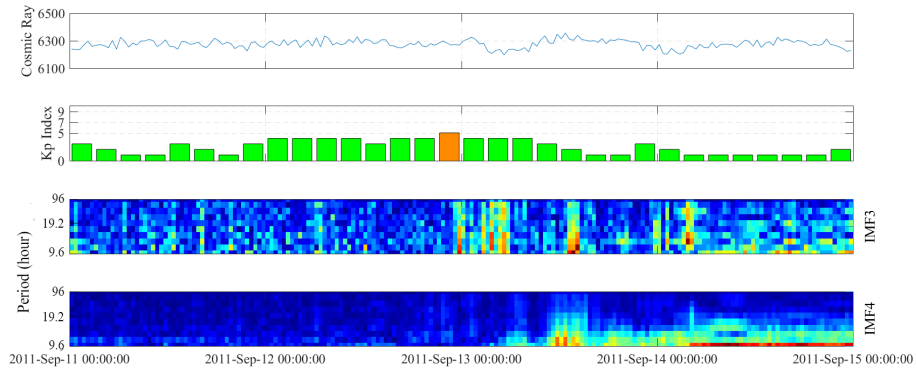(a)event on September 26, 2011 (b)event on September 7, 2017

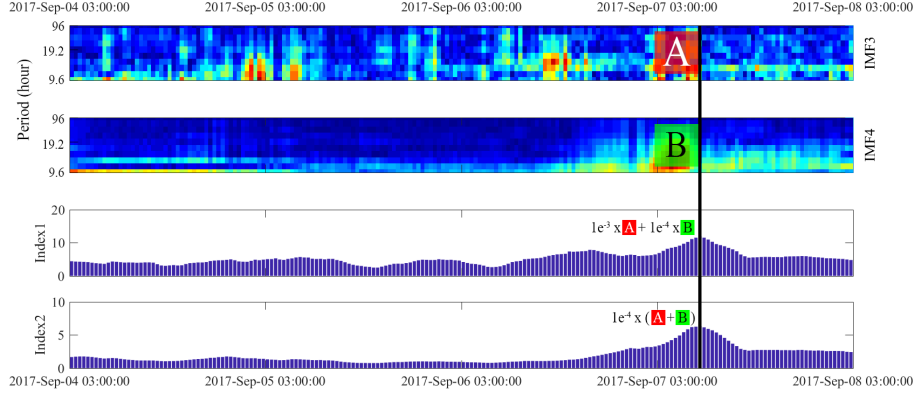Figure 5: Chain Reaction Caused by Geomagnetic Storm(Kp=5)

Figure 6: Construction Principle of Prediction Index

also why we construct two indices to track the fluctuation of GCR. The difference in order of magnitud means we can not simply add them together, so multiplying them with different coefficients makes them easier to add up.

The two cases above indicate why we need to focus on both IMF3 and IMF4 channels. If we just pay attention to IMF3, event1 is predicted accurately, but there would be some false positives before event2. Conversely, if we just focus on IMF4, event2 can be successfully forecasted, but event1 would be missed. Then two prediction indexes mentioned before is tested on event1 and event2. Figure 7(a) and 8(a) show the result. In both cases, enhancement in at least one index is appeared. For the sake of completeness of forecast, we also investigate the the quiet time of the same year with event1 and event2. Figure 7(b) and 8(b) show the quiet period in 2011 and 2017 respectively. Both indexes are much lower than storm period indeed.

As mentioned above, there are two precursors of our model. By using 11 selected events (list in Table 1) to verifying those two indexes, we find that most of geomagnetic storm (Kp≥8) are accurately forecasted. The detailed statistical results are shown in Table 2. The verification result turns out to be encouraging that nine-elevenths of study cases are predicted more than 9 hours in advance (accuracy: 82%).

5 Discussion

In this study, first improvement is combine signal decomposition and spectral analysis into one system. CEEMDAN is employed as signal decomposition method, which is based on EMD, and Hilbert Transform was chosen as the spectral analysis tool. Second improvement is transformation from 2D spectrum to 3D. Last improvement is two quantization indexes, which makes the relationship between GCRs and magnetic storms more intuitive. 11 CME cases from 1996 to 2018 were tested by our model. The result shows that two indexes constructed with GCR intensity can be a precursor of geomagnetic storm caused by CME. As summarized in Table2, there are 2 cases without any significant feature. According to the SOHO images, large area coronal hole existed on the solar surface before the occurence of geomagnetic storm. These coronal holes lead to geomagnetic storms(Kp≥5) both in the last and the next Carrington period. Therefor, the 2 failed cases were affected by these coronal holes. Maybe this is the reason why our model can't work. Beyond the 2 cases, 5 cases with warning sign in IMF3 or IMF4, and 4 cases with warning sign in both IMF3 and IMF4. Accuracy of our model is 82%. The conclusions are summarized below.
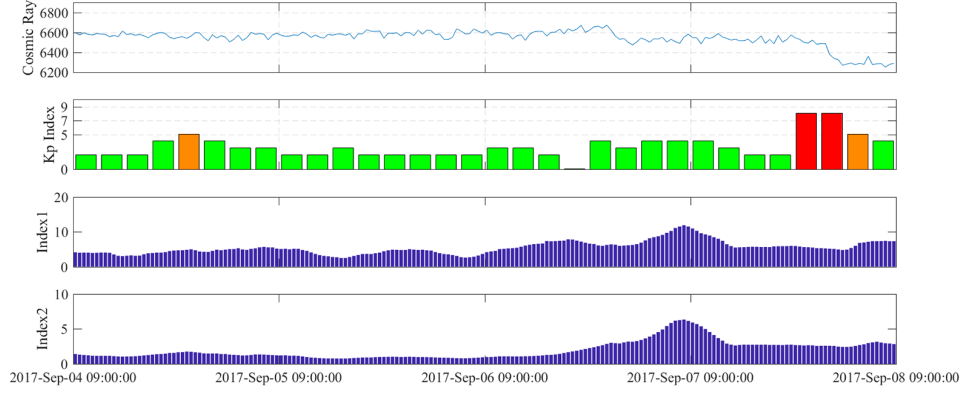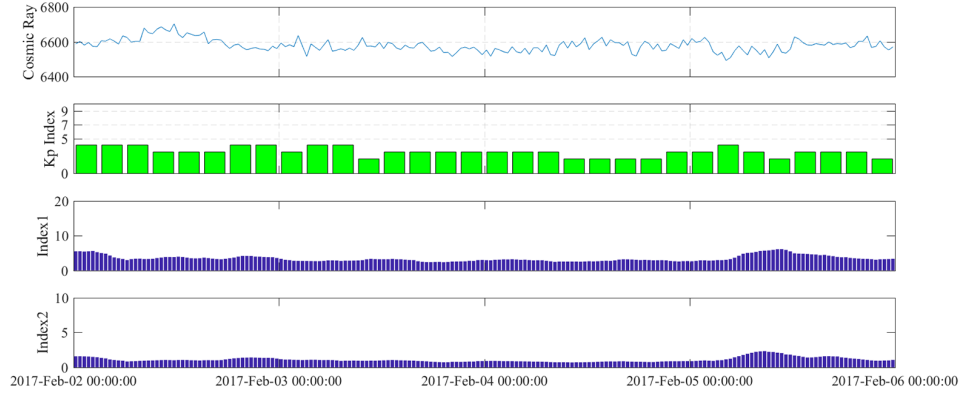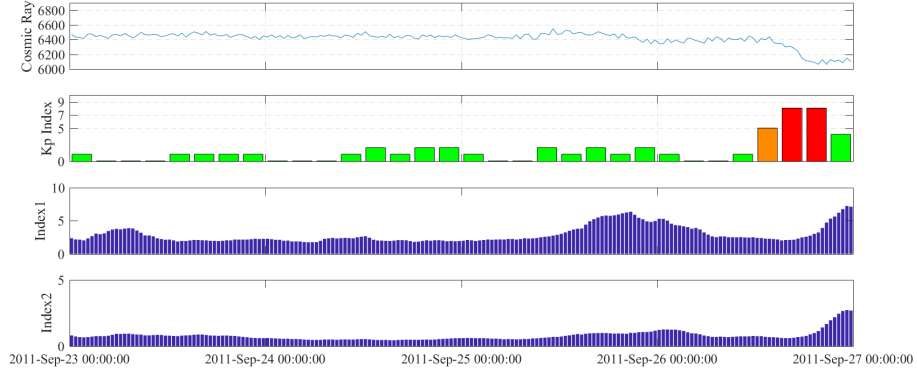
Figure 7: Indexes Variation during Storm Periods. GCRs, Kp index, Index1, Index2 are shown in turn from top to bottom.
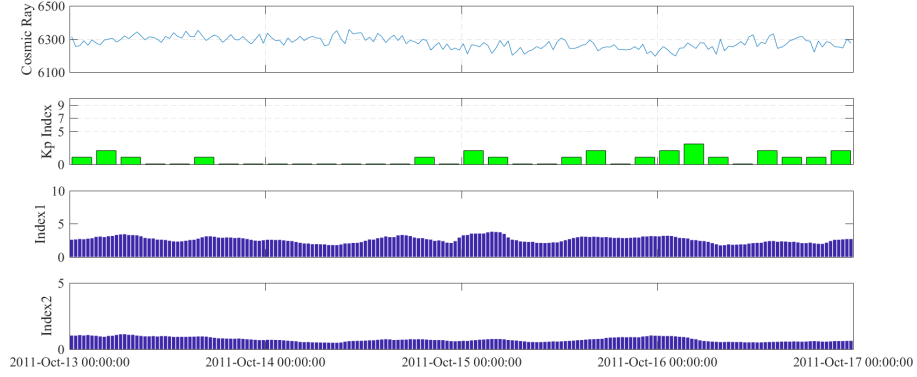(a)event on September 7, 2017 (b)Quiet Periods in the Same Year

1. As signal decomposition methods, CEEMDAN behaves more robust than EMD, it fixes frequency mixing problem and shows better anti-noise ability, both are important quality in forecasting application.

2. IMF3 and IMF4 are more sensitive to geomagnetic storms caused by CME, especially components with periods from 13 to 24 hours of them.

3. 3D Spectrum is an useful monitoring tool with comprehensive view, but not intuitive enough. Prediction indexes based on 3D spectrum takes forecasting work one step further.

4. Forecasting lead time calculated by our model ranges 9 to 24 hours, most of them are around 12 hours.

5. Except performance of prediction indexes during geomagnetic storms, we also check the their performance during quiet conditions, the results are shown in Figure7(b) and Figure8(b). In quiet period, both prediction indexes are much lower than storm period in the same year.

But there are still some unsolved problems. Firstly, it is hard to finding the definite value as the warning threshold in different years, which may be caused by the difference between solar cycles. Work of Otaola and Perez Enriquez (1983) indicates 5-year

(a)

(b)

Figure 8: Indexes Variation during Storm Periods. GCRs, Kp index, Index1, Index2 are shown in turn from top to bottom.
(a)event on September 26, 2011 (b)Quiet Periods in the Same Year

Table 2: The verification of prediction great geomagnetic storm

Date	Kp Index	Index1	Index2	Time in advance
2001-03-31	9	F	F	-
2001-11-24	9	T	T	9
2003-11-20	9	T	F	24
2004-11-07	9	T	T	12
2005-05-15	9	F	F	-
2005-08-24	9	T	F	24
2011-08-05	8	T	T	15
2011-09-26	8	T	F	15
2015-03-17	8	F	T	12
2015-06-22	8	T	F	12
2017-09-08	8	T	T	15

[a]T and F means predicted accurately or not.

variation is present during even cycles and absent in odd cycles, which may case inter-annual differences of GCRs. Introducing a fixing coefficient can fix this problem in the future. Secondly, amount of data is too small, because we have to choose storms only caused by CMEs, which is a tough requirement. Extending data volume and adding some new factors may solve this problem in the future.Hence,this method has a certain application prospect in geomagnetic prediction.

Acknowledgments

References

Barnhart, B. L., & Eichinger, W. E. (2011, Apr 01). Analysis of sunspot variability using the hilbert–huang transform. *Solar Physics*, *269*(2), 439–449. Retrieved from https://doi.org/10.1007/s11207-010-9701-6 doi: 10.1007/s11207-010-9701-6

Belov, A. V., Bieber, J. W., Eroshenko, E. A., Evensong, P., Pyle, R., & Yankee, V. G. (2003). Cosmic ray anisotropy before and during the passage of major solar wind disturbances. *Advances in Space Research*, *31*(4), 919-924.

Calogovic, J., Albert, C., Arnold, F., Beer, J., Desorgher, L., & Flueckiger, E. O. (2010). Sudden cosmic ray decreases: No change of global cloud cover. *Geophysical Research Letters*, *37*(3). Retrieved from https://agupubs.onlinelibrary.wiley.com/doi/abs/10.1029/2009GL041327 doi: 10.1029/2009GL041327

Cerrato, Y., Saiz, E., Cid, C., Gonzalez, W., & Palacios, J. (2012). Solar and interplanetary triggers of the largest dst variations of the solar cycle 23. *Journal of Atmospheric and Solar-Terrestrial Physics*, *80*, 111 - 123.

Chandorkar, M., Camporeale, E., & Wing, S. (2017). Probabilistic forecasting of the disturbance storm time index: An autoregressive gaussian process approach. *Space Weather-the International Journal of Research & Applications*, *15*.

Cho, I.-H., Cho, K.-S., Nakariakov, V. M., Kim, S., & Kumar, P. (2016, oct). COMPARISON OF DAMPED OSCILLATIONS IN SOLAR AND STELLAR x-RAY FLARES. *The Astrophysical Journal*, *830*(2), 110. Retrieved from https://doi.org/10.3847%2F0004-637x%2F830%2F2%2F110 doi: 10.3847/0004-637x/830/2/110

COLOMINAS, M. A., SCHLOTTHAUER, G., TORRES, M. E., & FLANDRIN, P. (2012). NOISE-ASSISTED EMD METHODS IN ACTION. *Advances in Adaptive Data Analysis*. doi: 10.1142/s1793536912500252

Coughlin, K. T., & Tung, K. K. (2004). 11-year solar cycle in the stratosphere extracted by the empirical mode decomposition method. *Advances in Space Research*, *34*(2), 323-329.

Dorman, L. I. (1999). Cosmic ray forbush-decreases as indicators of space dangerous phenomena and possible use of cosmic ray data for their prediction. *Proc Icrc*, *6*.

Dorman, L. I. (2005). Space weather and dangerous phenomena on the earth: principles of great geomagnetic storms forcasting by online cosmic ray data. *Annales Geophysicae*, *23*(9), 2997–3002. Retrieved from https://www.ann-geophys.net/23/2997/2005/ doi: 10.5194/angeo-23-2997-2005

Huang, N. E., Shen, Z., Long, S. R., Wu, M. C., Shih, H. H., Zheng, Q., ... Liu, H. H. (1998). The empirical mode decomposition and the hilbert spectrum for nonlinear and non-stationary time series analysis. *Proceedings: Mathematical, Physical and Engineering Sciences*, *454*(1971), 903–995. Retrieved from

345   `http://www.jstor.org/stable/53161`

346 Huang, N. E., & Wu, Z. (2008). *A review on Hilbert-Huang transform: Method and*
347   *its applications to geophysical studies.* doi: 10.1029/2007RG000228

348 Kichigin, G., Kravtsova, M., & Sdobnov, V. (2017). Parameters of current systems
349   in the magnetosphere as derived from observations of cosmic rays during the
350   june 2015 magnetic storm. *Solar-Terrestrial Physics*, *3*, 13-17.

351 Kilpua, E., Lugaz, N., Mays, M. L., & Temmer, M. (2019). Forecasting the structure
352   and orientation of earthbound coronal mass ejections. *Space Weather*, *17*(4),
353   498-526. Retrieved from `https://agupubs.onlinelibrary.wiley.com/doi/`
354   `abs/10.1029/2018SW001944` doi: 10.1029/2018SW001944

355 Kolotkov, D. Y., Anfinogentov, S. A., & Nakariakov, V. M. (2016). Empirical mode
356   decomposition analysis of random processes in the solar atmosphere. *Astron-*
357   *omy & Astrophysics*, *592*, A153.

358 Kravtsova, M. V., & Sdobnov, V. E. (2016). Cosmic rays during great geomag-
359   netic storms in cycle 23 of solar activity. *Geomagnetism & Aeronomy*, *56*(2),
360   143-150.

361 Kudela, K., Storini, M., Antalová, A., & Rybák, J. (2001). On the wavelet approach
362   to cosmic ray variability..

363 Kudela, K., Storini, M., Hofer, M. Y., & Belov, A. (2000). Cosmic rays in relation
364   to Space Weather. *Space Science Reviews*, *93*(1-2), 153–174. doi: 10.1023/A:
365   1026540327564

366 Käpylä, M. J., Käpylä, P. J., Olspert, N., Brandenburg, A., Warnecke, J., Karak, B.
367   B., & Pelt, J. (2016). Multiple dynamo modes as a mechanism for long-term
368   solar activity variations. *A&A*, *589*, A56. Retrieved from `https://doi.org/`
369   `10.1051/0004-6361/201527002` doi: 10.1051/0004-6361/201527002

370 Liu, L. B., & Wan, W. X. (2014). A brief overview on the issue on space physics and
371   space weather. *Chinese Journal of Geophysics*, *57*(11), 3493-3501.

372 Mandrikova, O., Polozov, Y., Fetisova, N., & Zalyaev, T. (2018). Analysis of the
373   dynamics of ionospheric parameters during periods of increased solar ac-
374   tivity and magnetic storms. *Journal of Atmospheric and Solar-Terrestrial*
375   *Physics*, *181*, 116 - 126. Retrieved from `http://www.sciencedirect.com/`
376   `science/article/pii/S1364682618301500` doi: https://doi.org/10.1016/
377   j.jastp.2018.10.019

378 Manninen, J., Kleimenova, N. G., Kozyreva, O. V., Ranta, A., Kauristie, K.,
379   Mäkinen, S., & Kornilova, T. A. (2008). Ground-based observations dur-
380   ing the period between two strong november 2004 storms attributed to steady
381   magnetospheric convection. *Journal of Geophysical Research: Space Physics*,
382   *113*(A3). Retrieved from `https://agupubs.onlinelibrary.wiley.com/doi/`
383   `abs/10.1029/2007JA012984` doi: 10.1029/2007JA012984

384 Munakata, K., Bieber, J. W., Yasue, S. I., Kato, C., Koyama, M., Akahane, S., . . .
385   Duldig, M. L. (2000). Precursors of geomagnetic storms observed by the muon
386   detector network. *Journal of Geophysical Research Space Physics*, *105*(A12),
387   27457-27468.

388 Otaola, J. A., & Perez Enriquez, R. (1983, Aug). Quasi-quinquennial variation
389   in cosmic ray intensity. In *International cosmic ray conference* (Vol. 10, p. 47-
390   50).

391 Otaola, J. A., Perez-Enriquez, R., & Valdes-Galicia, J. F. (1985, Aug). Difference
392   Between Even and Odd II-Year Cycles in Cosmic Ray Intensity. In *19th inter-*
393   *national cosmic ray conference (icrc19), volume 4* (Vol. 4, p. 493).

394 Shi, L. W., Shen, C. L., & Wang, Y. M. (2014). The interplanetary origins of ge-
395   omagnetic storm with dstmin ¡= -50 nt in 2007-2012. *Chinese Journal of Geo-*
396   *physics*, *57*(11), 3822-3833.

397 Stangalini, M., Consolini, G., Berrilli, F., Michelis, P. D., & Tozzi, R. (2014). Obser-
398   vational evidence for buffeting induced kink waves in solar magnetic elements.
399   *Astronomy & Astrophysics*, *569*.

Starodubtsev, S., Baishev, D., Grigoryev, V., Karimov, R., Kozlov, V., Korsakov, A., ... Moiseev, A. (2019). Analyzing solar, cosmic, and geophysical events in september 2017 using shicra sb ras complex observations. *Solar-Terrestrial Physics*, *5*, 14-27.

Starodubtsev, S. A., Grigoryev, V. G., & Gololobov, P. Y. (2019, Feb). Behavior of zonal components of cosmic ray distribution and Dst-index of geomagnetic field during periods of geoeffective disturbances of solar wind. In *Journal of physics conference series* (Vol. 1181, p. 012011). doi: 10.1088/1742-6596/1181/1/012011

Tokumaru, M., Fujiki, K., Iwai, K., Tyul'bashev, S., & Chashei, I. (2019, Jul 08). Coordinated interplanetary scintillation observations in japan and russia for coronal mass ejection events in early september 2017. *Solar Physics*, *294*(7), 87. Retrieved from https://doi.org/10.1007/s11207-019-1487-6 doi: 10.1007/s11207-019-1487-6

Tomassetti, N., Orcinha, M., Barão, F., & Bertucci, B. (2017). Evidence for a Time Lag in Solar Modulation of Galactic Cosmic Rays. *The Astrophysical Journal*, *849*(2), L32. Retrieved from http://dx.doi.org/10.3847/2041-8213/aa9373 doi: 10.3847/2041-8213/aa9373

Tsichla, M., Gerontidou, M., & Mavromichalaki, H. (2019). Spectral Analysis of Solar and Geomagnetic Parameters in Relation to Cosmic-ray Intensity for the Time Period 1965 – 2018. *Solar Physics*, *294*(1). Retrieved from http://dx.doi.org/10.1007/s11207-019-1403-0 doi: 10.1007/s11207-019-1403-0

Valdés-Galicia, J. F., Pérez-Enríquez, R., & Otaola, J. A. (1996, Aug). The Cosmic-Ray 1.68-Year Variation: a Clue to Understand the Nature of the Solar Cycle? *Solar Physics*, *167*(1-2), 409-417. doi: 10.1007/BF00146349

Wu, C.-C., Liou, K., Lepping, R. P., Hutting, L., Plunkett, S., Howard, R. A., & Socker, D. (2016, Sep 02). The first super geomagnetic storm of solar cycle 24: "the st. patrick's day event (17 march 2015)". *Earth, Planets and Space*, *68*(1), 151. Retrieved from https://doi.org/10.1186/s40623-016-0525-y doi: 10.1186/s40623-016-0525-y

Xiang, N. B., & Qu, Z. N. (2016, feb). ENSEMBLE EMPIRICAL MODE DECOMPOSITION OF THE MAGNETIC FIELD OF THE SUN AS a STAR. *The Astronomical Journal*, *151*(3), 76. Retrieved from https://doi.org/10.3847%2F0004-6256%2F151%2F3%2F76 doi: 10.3847/0004-6256/151/3/76

Xue, B. (2007). Preliminary attempt in prediction the geomagnetic storm with ground cosmic ray data. *Chinese Journal of Space Science*, *27*(3), 218-222.

Zhang, J., Richardson, I., Webb, D. F., Gopalswamy, N., Huttunen, E., Kasper, J., ... Wu, C. C. (2007). Solar and interplanetary sources of major geomagnetic storms (dst less than or equal to -100 nt) during 1996 - 2005. *Sociology & Anthropology*.

Zhu, X. L., Xue, B. S., Cheng, G. S., & Cang, Z. Y. (2015). Application of wavelet analysis of cosmic ray in prediction of great geomagnetic storms. *Chinese Journal of Geophysics*, *58*(7), 2242-2249.